



Impedance spectroscopy of monocrystalline silicon solar cells for photosensor applications: Highly sensitive device

A. Bouzidi^{a, **}, W. Jilani^{b,a}, I.S. Yahia^{c,d,e,*}, H.Y. Zahran^{c,d,e}

^a Research Unit, Physics of Insulating and Semi-insulating Materials, Faculty of Sciences, University of Sfax, B.P.1171, 3000, Sfax, Tunisia

^b Department of Physics, Faculty of Science Sciences and Arts Dhahran Al Janoub, King Khalid University, P.O. Box: 960 - Postal Code: 61421, Abha, Saudi Arabia

^c Research Center for Advanced Materials Science (RCAMS), King Khalid University, Abha 61413, P.O. Box 9004, Saudi Arabia

^d Advanced Functional Materials & Optoelectronic Laboratory (AFMOL), Department of Physics, Faculty of Science, King Khalid University, P.O. Box 9004, Abha, Saudi Arabia

^e Nanoscience Laboratory for Environmental and Bio-medical Applications (NLEBA), Semiconductor Lab., Metallurgical Lab.1, Department of Physics, Faculty of Education, Ain Shams University, Roxy, 11757 Cairo, Egypt



ARTICLE INFO

Keywords:

Monocrystalline silicon solar cell
Nyquist plots
Illumination conditions
AC impedance spectroscopy
Dielectric properties
Photosensor

ABSTRACT

In this study, the AC impedance measurements have been used to characterize the monocrystalline silicon solar cell device under dark and illumination conditions. AC impedance measurements in the illuminated conditions are analyzed to identify the electronic behavior through equivalent AC circuit representation in terms of lumped parameters obtained by fitting the measured impedance data. The angle impedance phase increases from negative to positive values with increasing illumination conditions. The real part Z' of the complex impedance value is typically higher at the dark light in the low-frequency region. It decreases gradually with increasing frequency reaching a plateau demonstrating independence on illumination at high frequencies. Nyquist plots exhibited a semicircle associated with the bulk single-crystalline body, and an additional spike is distinguishable at high frequency. The AC electrical conductivity is changed under dark and illumination conditions. Finally, the studied solar cell shows a highly sensitive light impedance response suggesting its suitability for use in photosensor applications.

1. Introduction

The solar or photovoltaic cell is a device that converts the sun, photons into electricity. It represents one of the most important renewable energy sources include hydroelectric power, solar energy, fuels derived from biomass, wind energy, and geothermal energy [1]. Generally, solar cells are produced from light-absorbing materials. If the cell is illuminated, optically generated carriers produce an electric current when the cell is connected to a load [2]. The high ratio of solar panel life and the emission of pollutants from the production process was desirable for renewable energy sources. This energy source can be generated locally, reducing energy distribution costs. Because of their attractive uses in microelectronic and optoelectronic applications such as organic film transistor and organic light-emitting diodes, organic semiconductor materials have recently been widely examined [3,4]. Silicon monocrystalline solar cells represent a reference in terms of

market share as well as performance in the photovoltaic ecosystem because it has several advantages like low maintenance cost, high reliability, noiseless and eco-friendly [5–7]. This is mostly attributable to the abundance and stability of silicon, and its relatively optimal properties.

Solar cell parameters, including short-circuit current, open-circuit voltage, efficiency, series resistance, shunt resistance, maximum output power, fill factor, and efficiency, are generally affected with cell temperature. The maximum influence is recorded in the open-circuit voltage due to light intensity and temperature variations [8]. Most silicon solar cells are designed to work under normal sunlight, and their performances are evaluated at 25 °C under AM-1.5 solar irradiation of 100 mW/cm² intensity [9]. A mismatch due to changes in the complex impedance can lead to a reduced performance of the total power generating system. Hence, for designing such efficient high-power photovoltaic systems, a detailed study on ac parameters of solar cells

* Corresponding author. Research Unit, Physics of Insulating and Semi-insulating Materials, Faculty of Sciences, University of Sfax, B.P.1171, 3000, Sfax, Tunisia.

** Corresponding author.

E-mail addresses: abdefatteh_bouzidi83@yahoo.fr (A. Bouzidi), isyahia@gmail.com, ihussein@kku.edu (I.S. Yahia).

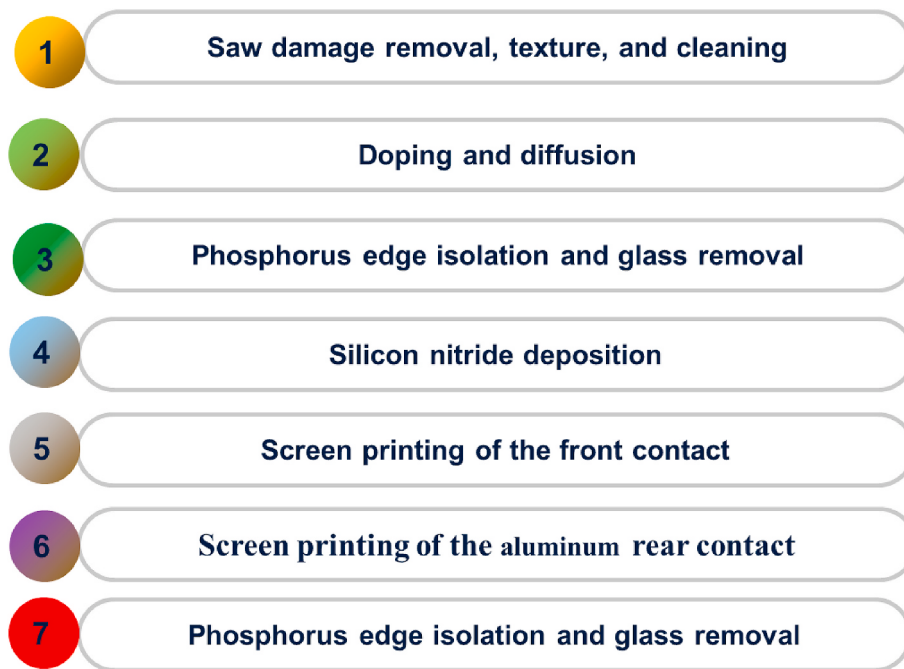


Fig. 1. Diagram of the preparation steps of monocrystalline silicon solar cell. (For interpretation of the references to colour in this figure legend, the reader is referred to the Web version of this article.)

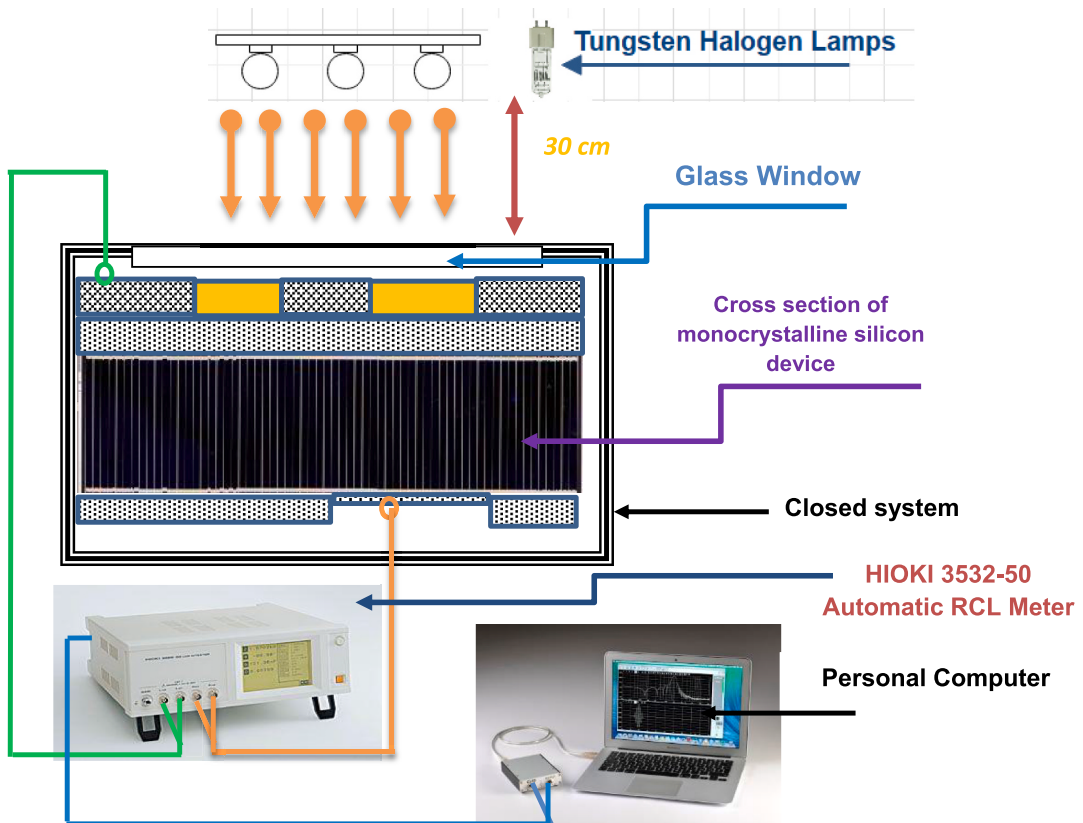


Fig. 2. Experimental setup system under dark and illumination conditions to quantity the AC impedance spectroscopy data.

is essential. In terrestrial applications, the solar cell is exposed to temperatures varying from 10 °C to 50 °C [10]. The AC parameters of a highly efficient commercial solar cell were measured at different cell temperatures by varying the cell bias voltage (forward and reverse) under dark conditions using impedance spectroscopy technique. It was

found that the cell capacitance increases with the temperature where the cell resistance decreases at any bias voltage [11].

Semiconductor solar cell materials are fundamentally quite simple devices. Semiconductors can absorb light and supplying electrical power to electrical electrons and holes as a part of absorbed photons.

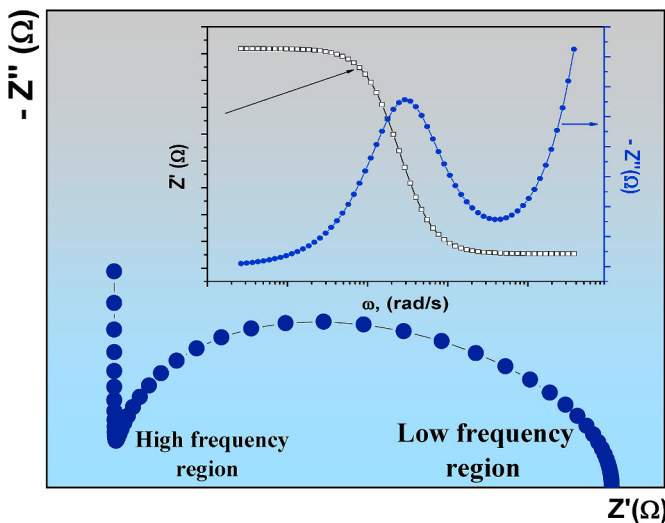


Fig. 3. The theoretical curve of the newly developed Eqs. (2&3).

Semiconductor structures in the nanometer scale are often critical to the current optoelectronic systems [12]. The source of electrical energy converted electrical current into optical signals is needed by semiconductor systems when light is used to transmit information. Photovoltaic technologies are part of the development of silicon solar cells, photochemical solar cells, and organic solar cells [13–15]. In a solar cell, the electron-hole pair can be separated by an electric field, which is usually recognized by a PN-junction. The electron-hole pair is making a statistical motion in a crystal so that the pair is very likely to enter the area where carriers are separated between the internal fields if their lifetime is long enough.

Impedance spectroscopy is commonly used for the study of operating mechanisms of different types of solar cells, such as inorganic, synthetic, organic, biological systems, dye-sensitized solar cells (DSC), organic solar cells and silicon solar cells. It also includes information on lifetimes, series and parallel resistances in groups, as well as on impurity densities of acceptors. It is made applying the AC voltage signal to a device and measuring the current through the materials. The impedance is usually measured in solar cells via a little AC enhancement signal and

a DC polarizing signal to pressure the cell's operating point. Solar cell DC parameters can either be measured with a frequency domain technology or a time-domain technique [16]. Different cell parameters, as series and parallel resistances, capacitance, diode factor, minority carrier lifetime, acceptor impurities density, and depletion layer charge density, have been obtained as a function of applied bias for different light illumination intensities. The behavior of cell capacitance under illumination is determined by the applied bias rather than by the light carrier generation when measurement at fixed bias is carried out [2].

An experimental setup to measure the AC parameters of solar cell devices were developed with a technique of impedance spectroscopy. The impedance spectrum of the device is represented by the imaginary and real parts of impedance in a complex plane with different frequencies. Impedance spectroscopy is mainly characterized by the measurement and analysis of some or all impedance related functions. The complex impedance $Z^*(\omega) = R(\omega) + jX(\omega)$ of a device is measured directly in an extensive range of frequency [17]. Here, $R(\omega)$ and $X(\omega)$ are the real and the imaginary part of the complex impedance, respectively. A purely sinusoidal voltage with different frequencies is applied to the device under test, and the phase shift and amplitude of the voltage and resultant current are measured. The ratio between the applied voltage and resultant current is calculated, and this is the impedance of the device under test [18]. The imaginary part versus real parts of the complex impedance (Nyquist plot) generally gives one or more features (mainly semicircles), depending on the number of mechanisms governing the device. Fitting and simulation, an electrical equivalent circuit provides parameters related to each feature (resistance and capacitance). A solar cell can be modeled as a parallel R - C network with series resistance.

In the present work, the impedance spectroscopy of monocrystalline silicon solar cells was investigated in detail under dark and illumination conditions in a wide frequency range from 42 Hz to 5 MHz at room temperature. The Nyquist plots and its related parameters are distinguishable and discussed in detail to have a wide-screen about the impedance behavior of the studied cell. Also, the equivalent circuit associated with the Nyquist plots for monocrystalline silicon taken in our account. Also, in this work, a new mathematical equation was developed and to describe the impedance behavior of the studied solar cell.

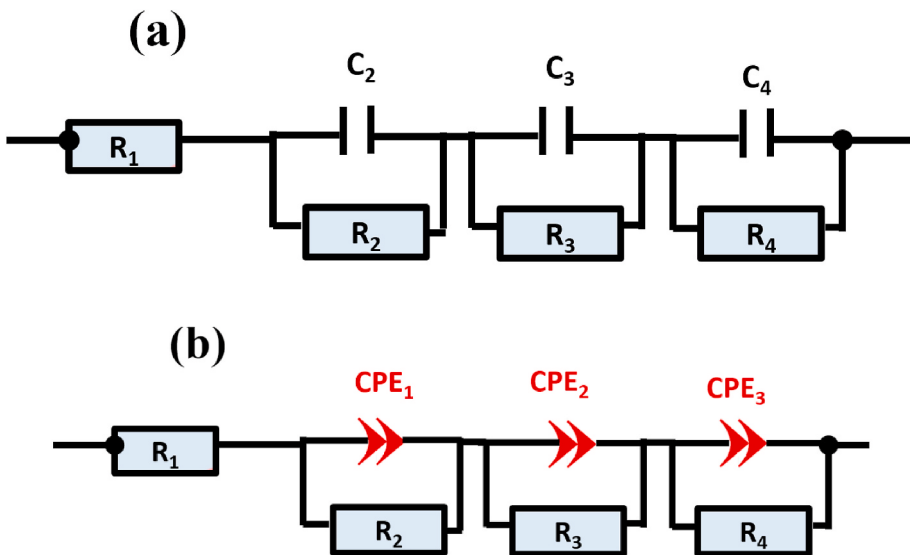


Fig. 4. (a,b). (a) The equivalent circuit for the monocrystalline silicon solar cell operating from dark to 5 mW/cm^2 , (b) Electric equivalent circuit used for fitting the impedance data for the studied specimen operating from 10 mW/cm^2 to 200 mW/cm^2 . (For interpretation of the references to colour in this figure legend, the reader is referred to the Web version of this article.)

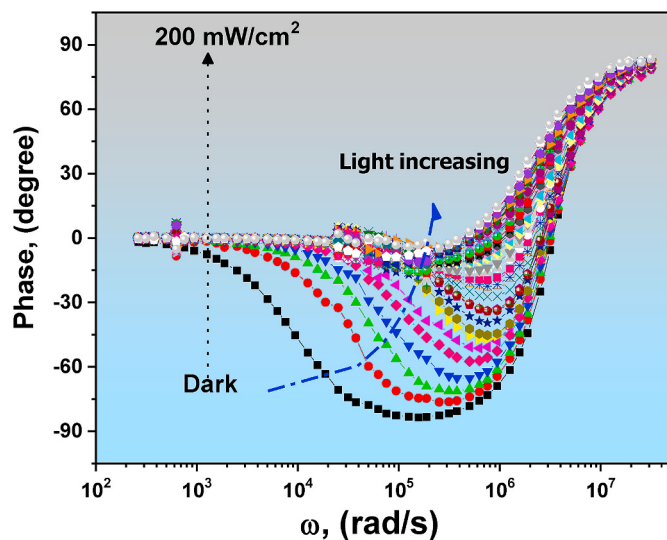


Fig. 5. Phase plots vs. the applied frequency under dark and different light illumination.

2. Experimental details

2.1. Solar cell monocrystalline silicon processing systems

The experimental preparation procedures of silicon energy solar monocrystalline cells are detailed and described based upon a very standardized process, which is forming a PN-junction [19,20]. The present solar cell device was grown in Solar Energy Factory, Arab International Optronics Co., Cairo, Egypt. Fig. 1 illustrates the mono-crystalline silicon solar cell fabrication process. All the steps involved in the fabrication of monocrystalline silicon solar cells are elaborately discussed in the sections of the published papers [19,20]. The total area of the silicon cell energy device equals 1.25 cm².

2.2. Calibration of the experimental setup

The complex impedance ($R + jX$ or $Z' + jZ''$) was performed with the help of HIOKI 3532-50 LCR Hi-Tester (Japan) for the standard monocrystalline silicon solar cells under both dark and illumination conditions at room temperature. All measurements are performed directly in the frequency domain over an extensive range of frequencies from 42 to 5 MHz attached to the specially designed holder. The holder was designed on Teflon sheets with two tungsten wires as a two-electrode (i.e., two probe measurements from upper and lower contacts of monocrystalline solar cells) to allow the light to penetrate the top surface of the studied cell. The bottom of the sample holder was made from copper brass sheets as a back contact. The calibrated and shielded cables of HIOKI 3532-50 LCR Hi-Tester are used in the setup to reduce any noise from the environment. These calibrated and shielded cables are directly connected to the two-probe holder without any extra connection cables.

A high-power tungsten halogen lamp, which produces a continuous spectrum of light from the ultraviolet region to the infrared region, i.e., 315–2000 nm, was used for the investigated measurements. For illumination, a calibrated high-power tungsten lamp was calibrated according to the solar simulator type (Solar Cell Tester M54A). The intensity of light was measured with a solar power meter (TM-206) and adjusted by changing the input power of the tungsten lamp. The voltage changes over the lamp resulted in the light intensity changes. The distance between the lamp and the sample is about 30 cm to avoid the thermal heating flow from the light source to the silicon solar cell device.

The experimental setup is shown in Fig. 2, and it was established to measure the complex AC impedance parameters of the monocrystalline silicon solar cell under dark and different illumination conditions. This

Figure consists of a closed system; automatic HIOKI 3532-50 LCR Hi-Tester is connected to a specially designed home-made holder, and personal computer whose impedance parameters are measured under dark and illumination conditions at room temperature with changeable of the applied frequency. The setup used here can be easily automated through computer control software.

2.3. Analytical approach

It was carried out an impedance analysis technique for separating the extrinsic polarization from bulk polarization. Impedance spectroscopy is a proven technique for the identification and differentiation of the dynamics of the different processes that govern the electrical response of the electronic/optoelectronic system devices. To understand the complex impedance behavior of the studied device, the measured data were used to estimate the parallel and serial combinations of an equivalent circuit model [21]:

$$Z(\omega) = Z'(\omega) + iZ''(\omega) \quad (1)$$

where ω is the angular frequency, Z' is the real part of impedance, and Z'' is the imaginary part of the impedance. In the present work, a new relationship based on the experimental plots of the real part of the impedance data is developed and given by Ref. [22]:

$$Z'(\omega) = R_1 + \frac{R_2}{1 + (\omega R_2 C_2)^2}, \quad (2)$$

Likewise, for the imaginary part of the impedance [23].

$$Z''(\omega) = -\frac{\omega R_3^2 C_3}{1 + (\omega R_3 C_3)^2} - \frac{\omega R_4^2 C_4}{1 + (\omega R_4 C_4)^2}, \quad (3)$$

where R_1 , R_2 , R_3 , and R_4 are resistances, C_2 , C_3 , and C_4 are capacities. The theoretical curve of the newly developed Eq. (2&3) is represented in Fig. 3.

2.4. The suggested equivalent electrical circuit model for the monocrystalline silicon solar cells

To interpret the set of results achieved in the present work, it is proposed a simple model, as shown in Fig. 4(a&b). The electrical behavior of the studied monocrystalline silicon device at different light conditions was fitted using an equivalent electric circuit, which is based on the combination of virtual R - C circuits attached with series resistance R_1 . In other words, a circuit like the hybrid Voight-matryoshka circuits-type circuit as proposed [24,25].

From dark to 5 mW/cm² illumination conditions, the bode impedance showed considerable changes as increasing the light intensities (see Fig. 4(a)) and the authors also reported the equivalent circuit parameters composed of a series resistor (R_1 denotes the ohmic resistance) with a series combination of parallel resistance-capacitance elements ($R_{2,3,4}$ denotes the polarization resistance, and $C_{2,3,4}$ denotes the polarization capacitance) for monocrystalline silicon sample test device. This suggestion is based on the symmetric Nyquist plots for the monocrystalline silicon device under dark and illumination conditions (i.e., from dark to 5 mW/cm²).

From 10 mW/cm² to 200 mW/cm² light illuminations, the authors proposed an equivalent circuit that simplified by removing capacitor elements as the capacitance, and the substrate is represented by a constant phase element (CPE) of the defined electric network at the bottom, as presented in Fig. 4(b) [26]. This kind of circuits is beneficial when two processes with different characteristic times are taking place simultaneously in the device. This suggestion is based on the asymmetric Nyquist plots for the monocrystalline silicon device under illumination conditions (i.e., from 10 to 200 mW/cm²).

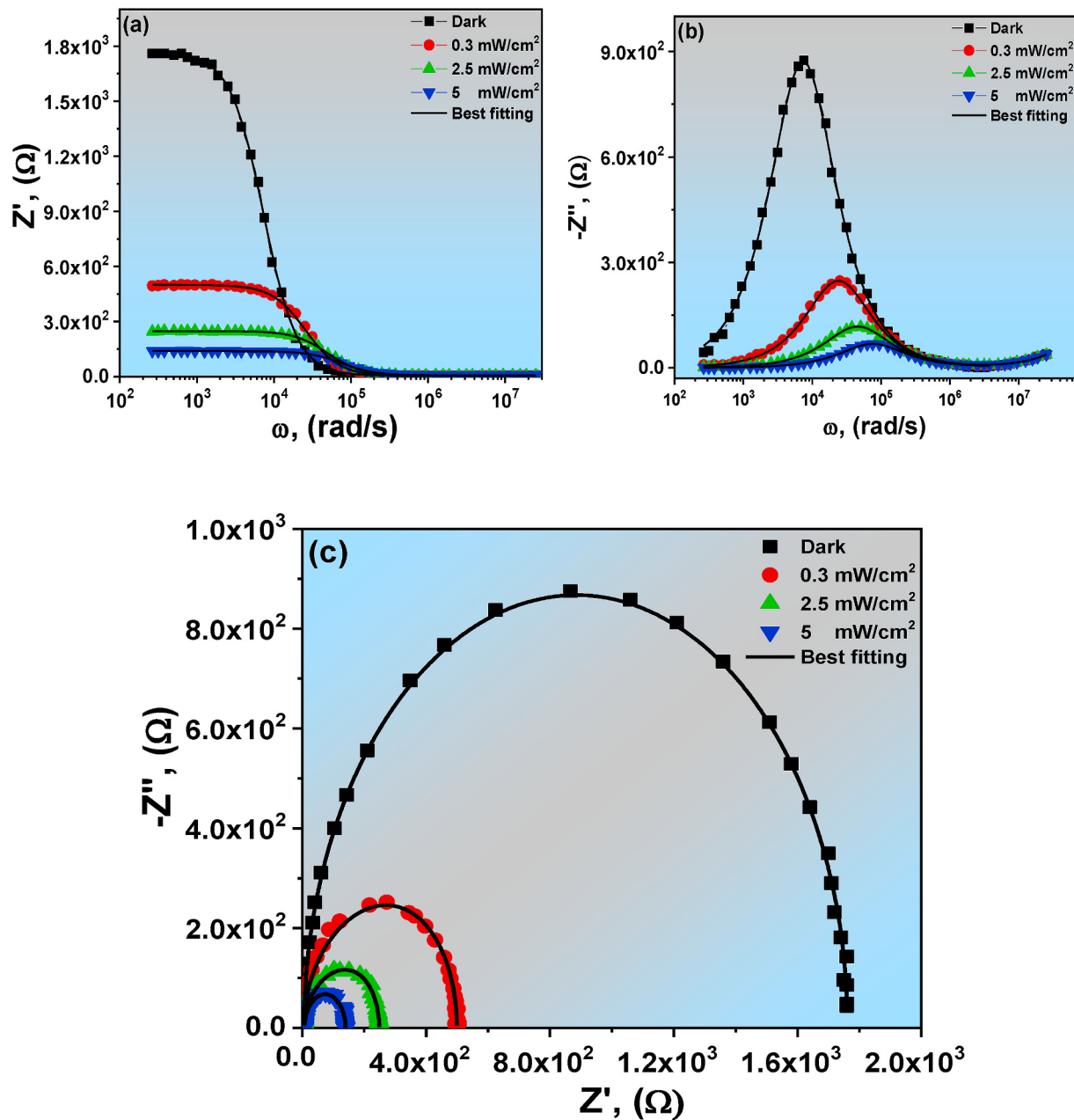


Fig. 6. (a-c). Real part (a) Imaginary part, (b) of the measured impedance spectra, and (c) Nyquist plot $-Z''$ & Z' of monocrystalline silicon solar cell from dark to 5 mW/cm^2 (The line represents the best fitting using the new Eqs. (2&3)). (For interpretation of the references to colour in this figure legend, the reader is referred to the Web version of this article.)

3. Results and discussions

3.1. Characteristics of phase spectra of the AC impedance

The phase plot for the monocrystalline silicon solar cell under dark and illumination conditions was shown in Fig. 5. At high-frequency region, the impedance phase spectra of monocrystalline silicon solar cell reached zero in the dark and with different illumination intensities, which due to the most resistive of the impedance. The phase curves of the impedance measurements shown in Fig. 5, have great discrimination between 10^3 Hz and 10^6 Hz, and that is why the phase can be used to estimate battery light illumination. The impedance angle increases from negative to positive values. This behavior reveals a major failure of the operation in photovoltaic devices. In the high frequency, strange behavior is seen due to the current and potential distribution of the

frequency. The effect of the light illumination on the phase angle is clearly defined and increased at the high-frequency region (above 10^6 Hz).

3.2. Impedance spectroscopy under dark and different illumination intensities

3.2.1. From dark to 5 mW/cm^2

The AC electrical behavior in various light illuminations of the solar cell system was modeled using a proposed electrical equivalent circuit based on electronic R-C circuits. The electric impedance analysis provides essential information about solar cell properties. It was used to evaluate serial/parallel resistance and transition/diffusion capacitance. Fig. 6(a-c) showed the real part, imaginary part spectra of the measured AC measured impedance, and the Nyquist plot of $-Z''$ & Z' of

Table 1

Data from the theoretical of the AC impedance using Eqs. (2&3) fitting values of the AC impedance using Eqs. (2&3) for monocrystalline silicon solar cells.

illumination conditions (mW/cm ²)	R ₁ , (Ω)	R ₂ , (Ω)	C ₂ , (F)	R ₃ , (Ω)	C ₃ , (F)	R ₄ , (Ω)	C ₄ , (F)
Dark	5.779	1755.9	7.74 × 10 ⁻⁸	1745.22	7.8 × 10 ⁻⁸	355.21	1.16 × 10 ⁻¹²
0.3	4.945	494.26	7.84 × 10 ⁻⁸	495.96	8.38 × 10 ⁻⁸	473.85	3.09 × 10 ⁻¹²
2.5	5.815	242.23	8.25 × 10 ⁻⁸	235.1	9.30 × 10 ⁻⁸	251.5	2.42 × 10 ⁻¹¹
5	7.149	132.04	9.98 × 10 ⁻⁸	136	9.72 × 10 ⁻⁸	548.57	5.04 × 10 ⁻¹²
10	5.369	76.51	5.27 × 10 ⁻⁷	54.72	6.16 × 10 ⁻⁷	687.52	2.07 × 10 ⁻¹¹
15	6.601	52.51	6.72 × 10 ⁻⁷	40.67	7.19 × 10 ⁻⁷	1220.19	6.6 × 10 ⁻¹²
20	6.442	37.82	7.19 × 10 ⁻⁷	31.2	8.6 × 10 ⁻⁷	655.38	2.3 × 10 ⁻¹¹
25	5.435	32.67	7.09 × 10 ⁻⁷	24.34	9.7 × 10 ⁻⁷	578.18	2.98 × 10 ⁻¹¹
30	6.630	26.37	7.66 × 10 ⁻⁷	18.82	1.36 × 10 ⁻⁶	543.18	3.39 × 10 ⁻¹¹
35	6.282	21.35	8.14 × 10 ⁻⁷	15.84	1.34 × 10 ⁻⁶	469.67	4.51 × 10 ⁻¹¹
40	5.982	19.75	8.21 × 10 ⁻⁷	11.85	1.56 × 10 ⁻⁶	1094.94	8.32 × 10 ⁻¹²
45	4.583	16.81	9.39 × 10 ⁻⁷	10.36	1.97 × 10 ⁻⁶	672.08	2.22 × 10 ⁻¹¹
50	5.576	13.85	1.08 × 10 ⁻⁶	8.28	2.83 × 10 ⁻⁶	196.62	2.67 × 10 ⁻¹⁰
55	5.227	11.87	1.24 × 10 ⁻⁶	4.95	4.20 × 10 ⁻⁶	241.58	1.75 × 10 ⁻¹⁰
60	4.90	12.05	1.27 × 10 ⁻⁶	5.86	3.94 × 10 ⁻⁶	261.94	1.49 × 10 ⁻¹⁰
65	5.47	10.27	1.49 × 10 ⁻⁶	5.57	5.37 × 10 ⁻⁶	175.66	3.38 × 10 ⁻¹⁰
70	5.31	9.90	1.45 × 10 ⁻⁶	4.02	3.67 × 10 ⁻⁶	393.31	6.59 × 10 ⁻¹¹
75	5.04	8.16	2.51 × 10 ⁻⁷	5.27	9.45 × 10 ⁻⁷	198.80	2.83 × 10 ⁻¹¹
80	4.95	7.79	2.51 × 10 ⁻⁷	4.81	1.33 × 10 ⁻⁶	132.83	7.67 × 10 ⁻¹¹
85	5.70	6.72	2.99 × 10 ⁻⁷	3.62	1.57 × 10 ⁻⁶	134.38	7.5 × 10 ⁻¹¹
90	5.94	6.41	3.46 × 10 ⁻⁷	3.01	1.70 × 10 ⁻⁶	123.14	9.01 × 10 ⁻¹¹
95	5.73	6.27	3.53 × 10 ⁻⁷	3.21	2.08 × 10 ⁻⁶	140.15	6.93 × 10 ⁻¹¹
100	5.27	5.37	4.86 × 10 ⁻⁷	3.95	2.47 × 10 ⁻⁶	125.84	8.66 × 10 ⁻¹¹
105	4.81	5.09	6.29 × 10 ⁻⁷	1.48	4.15 × 10 ⁻⁶	124.60	8.82 × 10 ⁻¹¹
110	4.48	4.35	7.14 × 10 ⁻⁷	0.21	5.46 × 10 ⁻⁸	117.98	9.98 × 10 ⁻¹¹
115	4.53	4.22	7.29 × 10 ⁻⁷	2.00	5.16 × 10 ⁻⁶	114.76	1.05 × 10 ⁻¹⁰
120	4.58	3.54	1.13 × 10 ⁻⁶	2.81	3.99 × 10 ⁻⁶	115.39	1.05 × 10 ⁻¹⁰
125	5.22	3.16	8.96 × 10 ⁻⁷	1.39	6.84 × 10 ⁻⁶	117.68	1.00 × 10 ⁻¹⁰
130	4.65	3.56	8.82 × 10 ⁻⁷	2.22	4.10 × 10 ⁻¹⁰	107.26	9.66 × 10 ⁻¹¹
135	4.82	3.45	1.77 × 10 ⁻⁶	0.42	3 × 10 ⁻⁵	255.4	1.97 × 10 ⁻¹¹
140	4.06	3.16	1.22 × 10 ⁻⁶	0.46	9 × 10 ⁻⁵	112.59	1.10 × 10 ⁻¹⁰
145	4.01	2.72	1.62 × 10 ⁻⁶	0.47	9.1 × 10 ⁻⁵	111.80	1.13 × 10 ⁻¹⁰
150	4.07	2.31	3.22 × 10 ⁻⁶	0.65	4 × 10 ⁻⁵	117.11	1.02 × 10 ⁻¹⁰
155	5.47	2.16	1.94 × 10 ⁻⁶	1.77	7.17 × 10 ⁻⁶	119.43	9.83 × 10 ⁻¹¹
160	5.01	2.48	3.17 × 10 ⁻⁶	0.96	2 × 10 ⁻⁵	111.35	1.13 × 10 ⁻¹⁰
165	4.34	2.26	1.57 × 10 ⁻⁶	1.74	1 × 10 ⁻⁵	115.85	1.05 × 10 ⁻¹⁰
170	4.34	1.93	2.35 × 10 ⁻⁶	1.44	9.2 × 10 ⁻⁶	163.28	5.11 × 10 ⁻¹¹
175	4.42	1.89	5.51 × 10 ⁻⁶	0.55	4 × 10 ⁻⁵	178.01	4.25 × 10 ⁻¹¹
180	4.55	1.79	2.25 × 10 ⁻⁶	0.72	5 × 10 ⁻⁵	338.68	1.14 × 10 ⁻¹¹
185	4.11	1.76	6.86 × 10 ⁻⁶	0.26	7 × 10 ⁻⁵	390.40	8.64 × 10 ⁻¹²
190	3.71	1.83	2.30 × 10 ⁻⁶	0.39	1.1 × 10 ⁻⁴	421.35	7.36 × 10 ⁻¹²
195	3.61	1.68	4.79 × 10 ⁻⁶	0.53	2.32 × 10 ⁻⁷	195.96	3.43 × 10 ⁻¹¹
200	3.55	1.48	3.26 × 10 ⁻⁶	0.28	1.94 × 10 ⁻⁷	122.26	8.96 × 10 ⁻¹¹

monocrystalline silicon from dark to 5 mW/cm² light illuminations, respectively.

Fig. 6(a) reveals, at various light illuminations, the real Z' component of the impedance as a function of frequency. From the plots in the low-frequency region, the amplitude Z' is higher and decreases monotonously as the frequency increases and remains constant at higher frequencies regardless of light illuminations. This may be due to the increase in AC conductivity with an angular frequency like that of semiconductor behaviors. The dispersion zone in the high-frequency region is observed with the increase in the light illumination. The decrease in Z' with the rise in the intensity of the angles can be induced because the material can be related to space charges by a slow dynamic relaxation process as compared to the dark in the superior angular frequency field. Impedance measurements on the silicon solar cell showed a decrease of the magnitude of Z' in its values with the increase of light illumination, which could be interpreted as the increase of the conductivity by photogenerated (excess) charge carriers. This may be due to the release of space charge polarization as a result of the lowering of the barrier properties of the solar cell materials. Similar results were reported by S. Nasri et al. [27]. Many other perovskite materials have already seen the same trend of Z' [28].

Fig. 6(b) indicates the frequency dependence at different light illumination conditions for the imaginary part of impedance Z'' for the monocrystalline silicon solar cell. With increasing the illumination conditions, the curves exhibit peaks marking the beginning of

conduction dispersion and relaxation processes. This result agrees with the reported by C. Zhai et al. [29]. In this figure, the Z'' values first increased and then decreased with increasing both the frequency and light illumination.

It should be noted that, with increased light illumination, the average peak position changes, and a broadening in the curves is observed with the decrease in peak height. If a p-n junction is illuminated, the semiconductor system produces additional electron-hole pairs. This broadening suggests spreading of relaxation time to the highest frequency, indicating a process of the relaxation time distribution in the solar cell system. These peaks showed a decreasing trend on increasing light illumination, indicating an increasing loss in the resistive property of the silicon solar cell systems.

Nyquist characteristics of the AC impedance from dark to 5 mW/cm² for monocrystalline silicon solar cells are shown in Fig. 6(c). The experimental impedance data are fitted into an equivalent circuit (see Fig. 4(a)). The equivalent circuit contained the following elements [30]. We have examined for the best fitting circuit about the shape of the frequency dependence of impedance spectra. As increasing the light illuminations (from dark to 5 mW/cm²), all obtained curves showed that there is the appearance of a single semi-circular arc indicating that the AC equivalent circuit of the studied solar cell consists of an R- and C- in parallel and attached with a series resistance R₁. Therefore, our fitting values are given in Table 1. The peak position of the relaxation peak shifts towards the higher frequency region with increasing the light

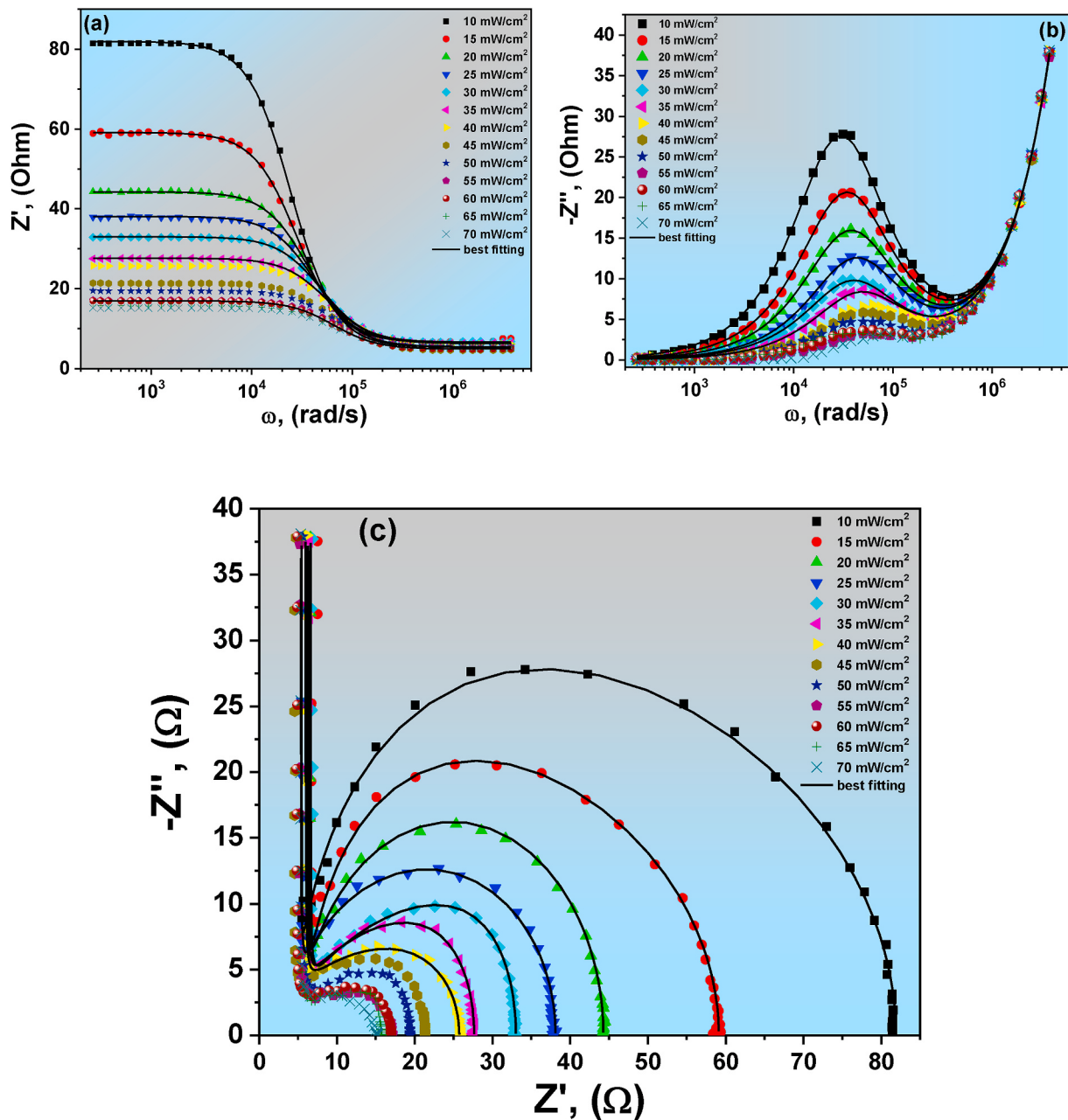


Fig. 7. (a-c). Real part (a), Imaginary part (b) of the measured impedance spectra, and (c) Nyquist plots $-Z''$ & Z' of monocrystalline silicon solar cell from $10 \text{ mW}/\text{cm}^2$ to $70 \text{ mW}/\text{cm}^2$ (The line represents the best fitting using the new Eq. (2&3)). (For interpretation of the references to colour in this figure legend, the reader is referred to the Web version of this article.)

illumination conditions. It is indicated that the relaxation process is light illumination dependent in the presently investigated monocrystalline silicon solar cell. The measured value R_1 ($R_1 = 5.779 \Omega$) for dark light of the monocrystalline silicon solar cells is confirmed and agreement by the reported and fitted value R_s obtained by S. Kumar et al. [22]. On the other hand, R_2 and C_2 exhibit opposite trends from dark to $5 \text{ mW}/\text{cm}^2$, where the value of the former is expected to be decreased, and the latter increased with the intensity of light. The observed increase in capacitance from dark to $5 \text{ mW}/\text{cm}^2$ illumination conditions can be explained by the A.R. Moore model [31]. The obtained values R_3 and C_3 showed the same trends in the illumination conditions from dark to $5 \text{ mW}/\text{cm}^2$.

3.2.2. From $10 \text{ mW}/\text{cm}^2$ to $70 \text{ mW}/\text{cm}^2$

The real, imaginary parts and Nyquist plots of $-Z''$ & Z' of monocrystalline silicon from in the light illuminations from $10 \text{ mW}/\text{cm}^2$ to 70

mW/cm^2 are shown in Fig. 7(a-c), respectively. The amplitude Z' is higher at low angular frequency region (see Fig. 7(a)) and decreases monotonously as frequency increases and remains constant at the higher frequencies regardless of increasing the light illumination conditions, which it is related to the increase in AC electrical conductivity with the rise of both the angular frequency and illuminations. The AC electrical conductivity of the monocrystalline silicon is changed under both dark and illumination conditions. The imaginary plot maintained at room temperature vs. angular frequency of monocrystalline silicon solar cell (see Fig. 7(b)) revealed a peak position under light illumination conditions at the medium angular frequencies and a spike at very high angular frequencies. The AC impedance experimental data were well fitted by using Eq. (2&3), from which the different values of R_i and the constant phase elements (CPE) instead of a normal capacitance C_i could be deduced, as gathered in Table 1. The Nyquist curve showed a variation

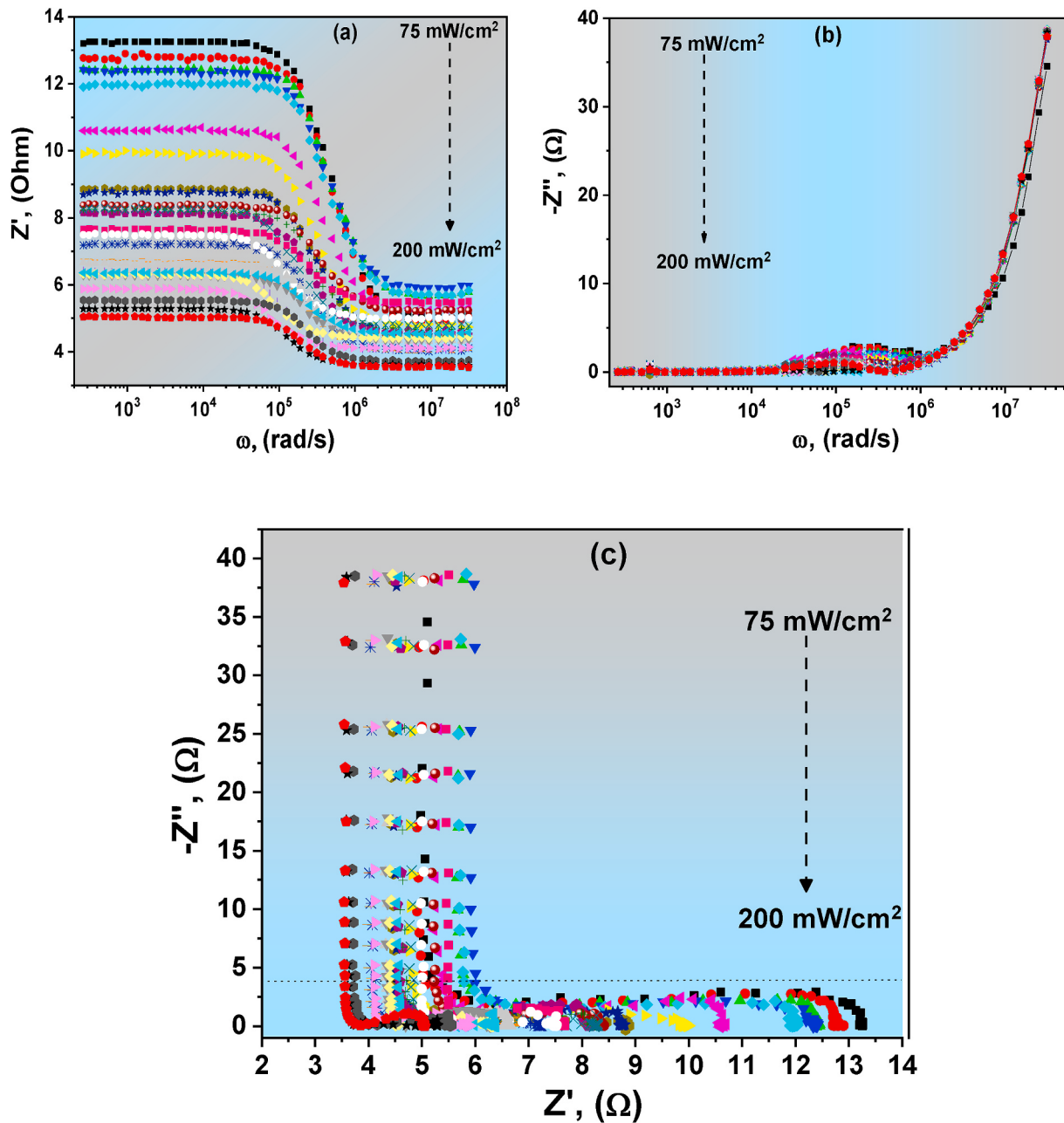


Fig. 8. (a-c). Real part (a) Imaginary part, (b) of the measured impedance spectra, and (c) Nyquist plot $-Z''$ & Z' of monocrystalline silicon solar cell from 75 mW/cm² to 200 mW/cm² (The line represents the best fitting using the new Eq. (2&3)). (For interpretation of the references to colour in this figure legend, the reader is referred to the Web version of this article.)

in both high and low frequencies, but at the low-frequency, the variations are dominants. The Nyquist plots (see Fig. 7(c)) exhibited a semicircle associated with the bulk single-crystalline body, and an additional spike is distinguishable at a very high-frequency region related to pure capacitor phenomenon. This result is agreed by Mark E. Orazem et al. [32]. The experimental impedance data were well fitted with an equivalent R - C circuit (see Fig. 4(b)) to elucidate this phenomenon. The equivalent circuit contained the following element parameters that were used in a similar previous work [33].

3.2.3. From 75 mW/cm² to 200 mW/cm² illumination conditions

The experimental data are presented in Fig. 8(a&b) for the real and imaginary parts of the impedance under illumination conditions from 75 mW/cm² to 200 mW/cm², respectively, for the monocrystalline silicon solar cell. The real impedance data were obtained similarly for the

other illumination conditions. The response of the real impedance is seen to be a healthy function of illumination conditions (see Fig. 8(a)). Therefore, our fitting values are added and gathered in Table 1. The Nyquist plots (see Fig. 8(c)) is fitted with an equivalent RC -circuit (see Fig. 4(b)). The Nyquist plots don't form exact semicircles; instead, they form depressed semicircles with their centers positioned below the x -axis as the illumination conditions increase. This figure showed a distinguishable spike in the high-frequency region, which is related to the pure capacitor phenomenon. The disappearance of semicircle gives the resistance value for the monocrystalline silicon solar cell is about 5 Ω, and the ideal capacitor is predominated under illumination conditions. The investigated sample behaves like an ideal capacitor.

The analysis of the obtained parameters in Table 1 showed the dependence of the resistance R_2 and R_3 values on the illumination conditions and decreased exponentially with increasing the illumination

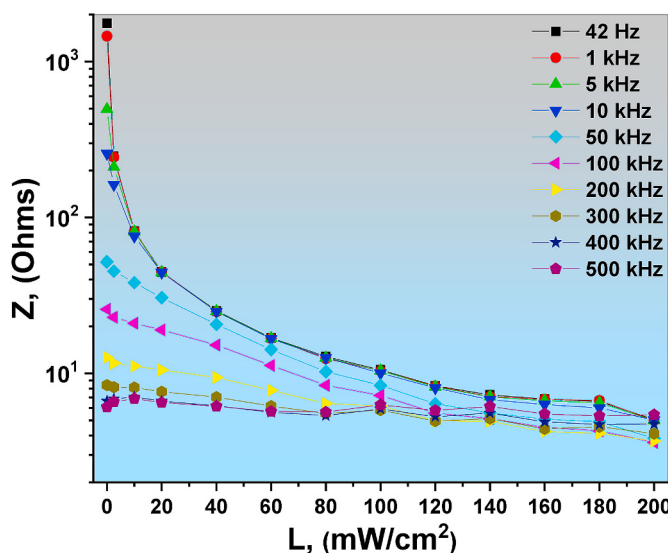


Fig. 9. Relation of the impedance of monocrystalline silicon solar cell vs. light illumination conditions at various frequencies. (For interpretation of the references to colour in this figure legend, the reader is referred to the Web version of this article.)

intensities for the measured sample. The obtained parameters change with light intensities. The values of R_2 is high under dark compared with its value under illumination conditions. The obtained resistance value after illumination conditions is smaller than the fitted value under dark light, which can be interpreted as a metal-semiconductor interface behavior.

Fig. 9 Shows the relation of the impedance of monocrystalline silicon solar cell vs. light illumination intensities at various frequencies. According to this Figure, the magnitude of the impedance increases for the applied frequencies at low light illumination. Meanwhile, at high illumination, it tends to decrease with an increase in the applied frequency. The impedance of the studied solar cells decreased with light illumination intensities, and with increasing the Applied frequencies, i.e., impedance values decreased. Such behavior supports the enhancement of the AC electrical conductivity of the studied devices under light and frequency.

4. Conclusion

In this study, experimental measurements using an AC impedance spectroscopy were carried out in the dark and different illumination intensities maintained at room temperature to investigate the effect of light illuminations on the dependent impedance parameters and their related equivalent AC circuit of the monocrystalline silicon solar cell specimen. The model shows a good agreement between the experimental AC impedance data and the calculated Nyquist plots. The analysis of the impedance showed that the phase angle increases from negative to positive values. The phase spectra of the impedance for the monocrystalline silicon solar cell under dark and illumination conditions at high frequencies reached zero, indicating that the impedance was mainly resistive. The real amplitude Z' is higher and decreased monotonously as the frequency increases and remains constant at the higher frequencies regardless of light illuminations. This may be due to the increase in the AC electrical conductivity with both angular frequency and light illumination intensity. The Nyquist plots exhibited a semicircle associated with the bulk monocrystalline body, and an additional spike is distinguishable at the high-frequency region, which related to the pure capacitor phenomenon. The proposed equivalent circuits are based on the Nyquist plots showed the necessary awareness of the operating mechanism of the fabricated sensor. The Nyquist plots

showed symmetric and asymmetric behaviors under dark and different illuminations intensities. The AC electrical conductivity of the monocrystalline silicon is changed under both dark and illumination conditions causes the high sensitivity light device, i.e., increased with increasing the light intensity. Monocrystalline silicon solar cells can be used extensively in a highly sensitive light sensor device for optoelectronic applications.

CRediT authorship contribution statement

A. Bouzidi: Conceptualization, Methodology, Software, Validation, Formal analysis, Investigation, Resources, Data curation, Writing - original draft, Writing - review & editing, Visualization. **W. Jilani:** Conceptualization, Methodology, Software, Validation, Formal analysis, Investigation, Resources, Data curation, Writing - original draft, Writing - review & editing, Visualization. **I.S. Yahia:** Conceptualization, Methodology, Software, Validation, Formal analysis, Investigation, Resources, Data curation, Writing - original draft, Writing - review & editing. **H.Y. Zahran:** Conceptualization, Methodology, Software, Validation, Formal analysis, Investigation, Resources, Data curation, Writing - original draft, Writing - review & editing, Supervision, Project administration, Funding acquisition.

Declaration of competing interest

All authors approved that there is no conflict of interest.

Acknowledgment

The authors express their appreciation to the Deanship of Scientific Research at King Khalid University for funding this work through research groups program under grant number R.G.P.2/38/40.

References

- [1] S. Chander, A. Purohit, A. Sharma, Arvind, S.P. Nehra, M.S. Dhaka, A study on photovoltaic parameters of mono-crystalline silicon solar cell with cell temperature, Energy Rep. 1 (2015) 104–109, <https://doi.org/10.1016/j.egyr.2015.03.004>.
- [2] K. Al Abdullah, F. Al Alloush, C. Salame, Investigation of the monocrystalline silicon solar cell physical behavior after thermal stress by AC impedance spectra, Energy Procedia 50 (2014) 30–40, <https://doi.org/10.1016/j.egypro.2014.06.004>.
- [3] Z.V. Vardeny, A.J. Heeger, A. Dodabalapur, Fundamental research needs in organic electronic materials, Synth. Met. 148 (2005) 1–3, <https://doi.org/10.1016/j.synthmet.2004.09.001>.
- [4] M. Yoshida, S. Uemure, T. Kodzasa, H. Ushijima, T. Kamata, High performance organic FET with double-semiconductor layers, Synth. Met. 137 (2003) 893–894, [https://doi.org/10.1016/s0379-6779\(02\)01129-3](https://doi.org/10.1016/s0379-6779(02)01129-3).
- [5] E. Cuce, P.M. Cuce, T. Bali, An experimental analysis of illumination intensity and temperature dependency of photovoltaic cell parameters, Appl. Energy 111 (2013) 374–382, <https://doi.org/10.1016/j.apenergy.2013.05.025>.
- [6] S.K. Sharma, H. Im, D.Y. Kim, R.M. Mehra, Review on Se-and S-doped hydrogenated amorphous silicon films, Indian J. Pure Appl. Phys. 52 (2014) 293–313.
- [7] P. Singh, N.M. Ravindra, Temperature dependence of solar cell performance-an analysis, Sol. Energy Mater. Sol. Cells 101 (2012) 36–45, <https://doi.org/10.1016/j.solmat.2012.02.019>.
- [8] T. Meng, C.M. Zhang, C. Liu, S.S. Meng, Experimental study of light intensity on I-V characteristic of single crystalline silicon solar cell, Adv. Mater. Res. 418–420 (2011) 725–1728. <https://doi.org/10.4028/www.scientific.net/AMR.418-420.1725>.
- [9] A.F. Braña, E. Forniés, N. López, B.J. García, High efficiency Si solar cells characterization using impedance spectroscopy analysis, J. Phys. Conf. Ser. 647 (2015), 012069, <https://doi.org/10.1088/1742-6596/647/1/012069>.
- [10] V. Schlosser, A. Ghitas, Measurement of silicon solar cells ac parameters. Proceedings of the Arab Regional Solar Energy Conference, Manama, Bahrain, Nov 2006.
- [11] R. Anil Kumar, M.S. Suresh, J. Nagaraju, Silicon (BSFR) solar cell AC parameters at different temperatures, Sol. Energy Mater. Sol. Cells 85 (2005) 397–406, <https://doi.org/10.1016/j.solmat.2004.05.017>.
- [12] J. Piprek, Introduction to Semiconductors, Semiconductor Optoelectronic Devices: Introduction to Physics and Simulation, Academic Press, San Diego, 2003.
- [13] M.A. Green, K. Emery, Y. Hishikawa, W. Warta, Solar cell efficiency tables (version 33), Prog. Photovoltaics Res. Appl. 17 (2009) 85–94, <https://doi.org/10.1002/pip.880>.

- [14] S. Günes, H. Neugebauer, N.S. Sariciftci, Conjugated polymer based organic solar cells, *Chem. Rev.* 107 (2007) 1324–1338, <https://doi.org/10.1021/cr050149z>.
- [15] C.J. Brabec, V. Dyakonov, J. Parisi, N.S. Sariciftci, *Organic Photovoltaics Concepts and Realization*, Springer, New York, 2003.
- [16] M.P. Deshmukh, R.A. Kumar, J. Nagaraju, Measurement of solar cell ac parameters using the time domain technique, *Rev. Sci. Instrum.* 75 (2004) 2732–2735, <https://doi.org/10.1063/1.1777380>.
- [17] R. Anil Kumar, M.S. Suresh, J. Nagaraju, Facility to measure solar cell ac parameters using an impedance spectroscopy technique, *Rev. Sci. Instrum.* 72 (8) (2001) 3422–3426, <https://doi.org/10.1063/1.1386632>.
- [18] M.P. Deshmukh, J. Nagaraju, Measurement of silicon and GaAs/Ge solar cell device parameters, *Sol. Energy Mater. Sol. Cells* 89 (2005) 403–408, <https://doi.org/10.1016/j.solmat.2005.01.005>.
- [19] O.A. Azim, I.S. Yahia, G.B. Sakr, Characterization of monocrystalline silicon solar cell, *Appl. Sol. Energy* 50 (2014) 146–155, <https://doi.org/10.3103/S0003701X14030037>.
- [20] I.S. Yahia, F. Yakuphanoglu, O.A. Azim, Unusual photocapacitance properties of a monocrystalline silicon solar cell for optoelectronic applications, *Sol. Energy Mater. Sol. Cell.* 95 (2011) 2598–2605, <https://doi.org/10.1016/j.solmat.2011.05.001>.
- [21] X.F. Wei, W.M. Grill, Impedance characteristics of deep brain stimulation electrodes in vitro and in vivo, *J. Neural. Eng.* 6 (2009), 046008, <https://doi.org/10.1088/1741-2560/6/4/046008>.
- [22] S. Kumar, P.K. Singh, G.S. Chilana, Study of silicon solar cell at different intensities of illumination and wavelengths using impedance spectroscopy, *Sol. Energy Mater. Sol. Cell.* 93 (2009) 1881–1884, <https://doi.org/10.1016/j.solmat.2009.07.002>.
- [23] W.R. Thurber, J.R. Lowney, R.D. Larrabee, J.R. Ehrstein, AC impedance method for high-resistivity measurements of silicon, *J. Electrochem. Soc.* 138 (1991) 3081–3085, <https://doi.org/10.1149/1.2085372>.
- [24] R.S. Sanchez, V. Gonzalez-Pedro, J.-W. Lee, N.-G. Park, Y.S. Kang, I. Mora-Sero, J. Bisquert, Slow dynamic processes in lead halide perovskite solar cells. Characteristic times and hysteresis, *J. Phys. Chem. Lett.* 5 (2014) 2357–2363, <https://doi.org/10.1021/jz5011187>.
- [25] A. Todinova, L. Contreras-Bernal, M. Salado, S. Ahmad, N. Morillo, J. Idígoras, J. A. Anta, Towards a universal approach for the analysis of impedance spectra of perovskite solar cells: equivalent circuits and empirical analysis, *Chem. Electro. Chem.* 4 (2017) 2891–2901, <https://doi.org/10.1002/celc.201700498>.
- [26] K.P. Ramaiyan, J.A. Pihl, C.R. Kreller, V.Y. Prikhodko, S. Curran, J.E. Parks, R. Mukundan, E.L. Brosha, Response characteristics of a stable mixed potential ammonia sensor in simulated Diesel exhaust, *J. Electrochem. Soc.* 164 (9) (2017) B448–B455, <https://doi.org/10.1149/2.1271709jes>.
- [27] S. Nasri, A.L. Ben Hafsa, M. Tabellout, M. Megdiche, Complex impedance, dielectric properties and electrical conduction mechanism of $\text{La}_{0.5}\text{Ba}_{0.5}\text{FeO}_{3-\delta}$ perovskite oxides, *RSC Adv.* 6 (2016) 76659–76665, <https://doi.org/10.1039/C6RA10589K>.
- [28] A. Benali, A. Souissi, M. Bejar, E. Dhahri, M.F.P. Graça, M.A. Valente, Dielectric properties and alternating current conductivity of sol-gel made $\text{La}_{0.8}\text{Ca}_{0.2}\text{FeO}_3$ compound, *Chem. Phys. Lett.* 637 (2015) 7–12, <https://doi.org/10.1016/j.cplett.2015.07.041>.
- [29] C. Zhai, Y. Gan, D. Hanaor, G. Proust, stress-dependent electrical transport and its universal scaling in granular materials, *Extreme Mech. Lett.* 22 (2018) 83–88, <https://doi.org/10.1016/j.eml.2018.05.005>.
- [30] S. Sureshkumar, B. Venkatachalamapathy, T.M. Sridhar, Enhanced H_2S gas sensing properties of Mn doped ZnO nanoparticles – an impedance spectroscopic investigation, *Mater. Res. Express* 6 (2019), 075009, <https://doi.org/10.1088/2053-1591/ab0eef>.
- [31] A.R. Moore, Solar cell capacitance, *RCA Rev.* 36 (1975) 551–565.
- [32] M.E. Orazema, B. Tribollet, An integrated approach to electrochemical impedance spectroscopy, *Electrochim. Acta* 53 (2008) 7360–7366, <https://doi.org/10.1016/j.electacta.2007.10.075>.
- [33] V. Balasubramani, S. Chandraseka, T. Subba Rao, R. Sasikumar, M.R. Kuppusamy, T.M. Sridhar, Review—Recent advances in electrochemical impedance spectroscopy based Toxic gas sensors using semiconducting metal oxides, *J. Electrochem. Soc.* 167 (2020), 037572, <https://doi.org/10.1149/1945-7111/ab77a0>.